Drill-exit temperature characteristics in drilling of UD and MD CFRP composites based on infrared thermography

International Journal of Machine Tools and Manufacture 135 (2018) 24–37

Contents lists available at ScienceDirect

International Journal of Machine Tools and Manufacture

journal homepage: www.elsevier.com/locate/ijmactool

Drill-exit temperature characteristics in drilling of UD and MD CFRP composites based on infrared thermography

Rao Fu[a,b], Zhenyuan Jia[a,*], Fuji Wang[a], Yan Jin[b], Dan Sun[b], Lujia Yang[c], De Cheng[a]

[a] Key Laboratory for Precision and Non-traditional Machining Technology of Ministry of Education, School of Mechanical Engineering, Dalian University of Technology, Dalian, 116024, PR China

[b] School of Mechanical and Aerospace Engineering, Queen's University Belfast, Belfast, BT9 5AG, United Kingdom

[c] School of Innovation and Entrepreneurship, Dalian University of Technology, Dalian, 116024, PR China

ARTICLE INFO

Keywords:
Drilling of CFRP
Temperature characteristics
Thermal image
Temperature effects
Drilling qualities

ABSTRACT

This paper presents a comprehensive study on the complex drill-exit temperature characteristics in the drilling of unidirectional (UD) and multidirectional (MD) CFRPs using a state-of-art microscopy infrared imaging system. For the first time, temperature variation and distribution at drill exit have been revealed in full detail, associated with the CFRP material properties and drilling conditions. Results suggest that the actual drill/CFRP interactions have critical but similar effects on the drill-exit temperatures for UD and MD CFRPs. Specifically, three distinct cutting regions with varying temperature characteristics are evident when the main cutting edge is acting on the drill exit material. In all cases, the temperature distribution features elliptical shape, of which the eccentricity depends on the lay-up sequence and the drilling depth. In addition, the real-time temperature profiles and 2D/3D maximum temperature distribution maps are created with high visualization. With the aid of those findings, the relationships between drilling temperature maxima, their locations and drilling depths have been discovered and temperature effects on drill-exit damages have been elucidated for the first time. MD CFRP is proven more difficult to achieve high drilling qualities at certain fiber cutting angles than UD CFRP due to the associated temperature effects. Such important knowledge enables the identification of the heat affected zones and subsequently informs strategies for reducing the negative temperature effects.

1. Introduction

Due to their superior specific strength/stiffness and excellent fatigue resistance, carbon fiber reinforced polymer/plastic (CFRP) composites are highly favorable in the manufacturing of lightweight components with enhanced structural efficiency in the fields of aerospace, transportation and energy, etc. The global market growth of CFRP is predicted to be $25.2 billion by 2020, and manufacturers are constantly seeking solutions for cost effective production of CFRP components with repeatable high quality [1]. Although most CFRP components could be fabricated in near net shape via prepreg lay-up and autoclave processes, secondary machining processes such as drilling and trimming are still necessary to achieve geometric and dimensional tolerances for effective joining and assembly. However, CFRP belongs to hard-to-machine materials and is particularly sensitive to high temperatures. The machining process of CFRP is typically performed in a dry condition, as traditional coolants usually interact with CFRP physically and/or chemically, leading to undesirable machining errors and weakened material bearing capacity [2–4]. Due to its low thermal conductivity and low specific heat capacity, heat can easily accumulate in CFRP cutting zone in the absence of coolant. Particularly, in traditional drilling [3] as well as ultrasonic drilling of CFRP [5], the relatively enclosed manufacturing environment with poor ventilation is inevitable and will always lead to a rapid increase of the temperature, probably exceeding the glass transition temperature (T_g) of CFRP (approximately 160–200 °C) [6–8]. As a result, the high temperature in CFRP machining would soften the resin matrix [3,9] and even results in thermal degradation during a short aging period, compromising the CFRP mechanical properties [10–13]. In addition, the drill exit of a hole, subjected to large deflection without back support and constraint, is the most susceptible area to damages such as delamination, splintering and burr. Unfortunately, the cutting temperature usually reaches the maxima at the CFRP drill exit [4,7]. This further worsens the drill-exit damages [14] and the serious drilling damages will also degrade the

* Corresponding author.
E-mail addresses: r.fu@qub.ac.uk (R. Fu), jzyxy@dlut.edu.cn (Z. Jia), wfjsll@dlut.edu.cn (F. Wang), y.jin@qub.ac.uk (Y. Jin), d.sun@qub.ac.uk (D. Sun), ylj@dlut.edu.cn (L. Yang), 496268126@qq.com (D. Cheng).

https://doi.org/10.1016/j.ijmachtools.2018.08.002
Received 28 March 2018; Received in revised form 1 August 2018; Accepted 6 August 2018
Available online 09 August 2018

mechanical properties of the machined CFRP components [15,16]. Those direct and indirect negative effects of high drilling temperatures have brought great challenges to quality control. Given the existing challenges, a thorough understanding of the CFRP drill-exit temperature characteristics and their effects on drilling qualities is urgently required. The in-depth knowledge will enable effective evaluation and optimization of the drilling process, inform the design and analysis of composites and cutting tools, and advance the future CFRP manufacturing technology towards greater manufacturing efficiency and cost reduction.

Due to its complex structure, the cutting temperature characteristics of CFRP cannot be determined using existing protocols for metal cutting [17–19]. The specific manufacturing processes of CFRP composites, such as stacking prepregs or fiber bundles in designed sequences and directions, have resulted in their anisotropic structures and properties. More specifically, the reinforcing carbon fiber has a much better thermal conductivity than the resin matrix, hence the heat accumulation during cutting mostly occurs in the resin matrix. The thermal conduction processes of the stacking layers are also vastly different in the longitudinal (along fiber) and transverse (cross fiber) directions [20–22], and the temperature characteristic in the cutting of each layer is pertinent to the fiber cutting angle [23,24]. In particular, for MD CFRP that consists of multi-directional layers (e.g. 0°, 45° or 90° fiber orientation in adjacent layers), the heat conduction mechanisms during cutting operation are even more complicated [21,22].

To date, the investigations into the effects of complex CFRP structures/properties on the drill-exit temperature characteristics and consequently the hole qualities, are still in infancy. Different approaches, such as theoretical, simulation and experiment-based studies have been attempted to acquire temperature characteristics in the drilling of CFRP. Liu et al. [25] conducted leading work in building theoretical models for predicting the cutting temperature in the helical milling of unidirectional (UD) CFRP holes. However, the complex interactions between layers with different fiber orientations like multidirectional (MD) CFRP and the actual drill/CFRP cutting interactions under large deflections [26] are yet to be considered for a more accurate and universal model. On the other hand, Zhu et al. [27] and Sadek et al. [28] demonstrated preliminary simulation results for the drilling-exit temperature characteristics in the drilling of UD and MD CFRPs. The percentage of cutting energy (defined as the heat partition ratio flowing into the workpiece) is critical for the accuracy of the simulation results [29]. However, it is affected instantaneously by the time-dependent fiber cutting angle [30] and the distinct mode of material removal induced by the serious deflection at drill exit [26]. As a result, the current prediction on heat transfer has a large uncertainty and the results may severely deviate from the drilling processes in practice.

The experiment-based approach is considered to be more reliable as temperature characteristics in CFRP drilling can be revealed through direct measurements in the targeted areas. Contact measurement methods commonly include the use of thermocouples, optical fiber sensors, etc. [18,19,31], whereas infrared thermography [32,33] has been explored for non-contact measurement of temperatures with the infrared camera. In the drilling of CFRP, researchers have employed embedded thermal sensors on the flank faces of drills to monitor the temperature with varying processing parameters [3,6,34,35]. Due to the unique thermal properties of tool material and CFRP, and different heat distributions in tool, workpiece and chips, the measured temperature can only represent the average temperature within a wide zone rather than the specific temperature of the machined surface. In other cases, thermocouples were embedded both inside and outside the hole periphery for temperature detection at the tool-workpiece interface, or placed outside the hole to capture the temperature characteristics of the overall CFRP drilling process [7,9,14,24,36]. However, as the sensor's position is much restricted spatially by the experiment layout, it is difficult to obtain sufficient and accurate temperature data to reveal the comprehensive temperature characteristics at drill exit. In comparison, infrared thermography is capable of acquiring complete temperature data within a large detection area, which enables offline data processing/analysis [19]. The reliability of such technology has been verified in several studies with simultaneous thermocouple measurements during the CFRP machining processes [31,36,37].

Furthermore, the studies on the CFRP drilling temperature with the infrared camera have mostly focused on the general temperature distributions at the drill exit [27,28,38] and drill entrance [39], as well as the basic temperature changing regularities along with drilling parameters [40] and the hole radius [36]. Recently, drilling delamination has been associated with thermal effects [41]. These studies have provided some useful and preliminary results for the drilling temperature investigations of CFRP. However, the studies suffer from low spatial resolution (about several hundred micrometers per pixel) or insufficient frame frequency (below 100 Hz) of the thermal imaging system, and thermal data lack post processing for further analyses. These limitations make it impossible to capture/visualize many important fine details of temperature characteristics which are associated with the high-speed machining process, actual drill/CFRP cutting interaction, fiber cutting angle and lay-up sequence, etc. Consequently, not in-depth conclusions have been drawn and some even remain controversial, e.g., the average temperatures of the entire drilling area have been used for analyses, however, the temperature origins from uncut materials, cutting tool or chips have not been justified. Therefore, the drill-exit temperature characteristics in the drilling of CFRP and the associated effects on drilling qualities are yet to be revealed.

This paper presents a comprehensive experimental study on the complex temperature characteristics at drill exit in the drilling of UD and MD CFRPs based on infrared thermography. A high resolution microscopic infrared imaging system has been deployed to capture the dynamic drilling process under a high frame frequency. For the first time, temperature variation and distribution at drill exit are revealed in full detail and the results are associated with the CFRP material properties and drilling conditions (e.g. drilling depths, cutting interactions and fiber cutting angles). Furthermore, with high visualized temperature characteristics, relationships between drilling temperature maxima, their locations and drilling depths have been established to help identify the potential heat affected zones. Finally, the impact of adjacent layers of UD and MD CFRPs on the resulting temperature characteristics has been studied, and their subsequent effects on the drill-exit qualities have been elucidated. The methodology proposed in this paper can be widely applied in the investigation of machining temperature characteristics of many other material systems.

2. Methods

2.1. Temperature measurement methodology

Temperature characteristics during the dynamic drilling process were captured using a Telops-MW infrared camera with a Stirling Cooling system to achieve low-noise thermal images under a high frame frequency. A calibrated lens extender was used to optically enlarge the area of observation and enable the microscale analysis. A special CaF_2 cover (transmittance 93% for the infrared radiation) was installed to protect the infrared lens. The thermal imaging system has been calibrated by blackbody free calibration technique [42] to minimize the effects of the ambient environment, and its error is within 1% between −15 °C and 324 °C. Note that the true accuracy of the thermal imaging system can be affected by numerous factors [32] and can vary with different materials used in tests. To address this issue, CFRP temperatures were controlled in a thermostatic chamber, and the parameters of the thermal imaging system were adjusted against the results obtained from a high precision K-type thermocouple (Omega GG-K-36, error 0.75%) under the same drilling condition. The detail parameters are listed in Table 1. Results for the employed CFRP indicate that temperatures measured by this thermal imaging system were within ± 5%

Table 1
Parameters of thermal imaging system deployed in this study.

Parameter	Temperature range (°C)	Spectral range (μm)	Image format (pixel)	Spatial resolution (μm/pixel)	Image frequency (Hz)	Emissivity
Value	−15 to 324	3.8 to 4.9	256 × 256	43	300	1

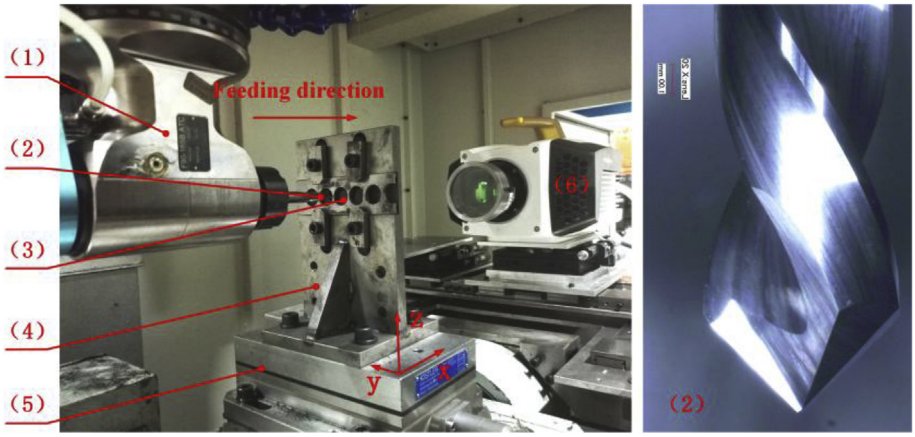

Fig. 1. Experimental layout (1. 90° angle head, 2. small point angle twist drill, 3. CFRP workpiece, 4. fixture, 5. force dynamometer, 6. infrared camera).

deviation of the thermocouple data. Unfortunately, the temperature of the tool cutting edge cannot be measured accurately, as it is affected by the strong reflections at the smooth surfaces (e.g. rake face, flank face etc.) [32]. Meanwhile, due to the complex structure of the cutting edge, this cannot be rectified by adjusting the infrared camera parameters. Therefore, this study has been focused on capturing temperature data of CFRP during the drilling process, and the recorded data have been processed for further analyses.

2.2. Drilling experiment setup

Lateral drillings were adopted for the direct observation of the drill exit through the infrared camera. Fig. 1 shows the experimental layout. Drilling experiments were carried out in a vertical CNC machining center. A 90° angle head (1) was installed on the spindle, which enabled the drill (2) mounted on the angle head to feed along the X axis in the coordinate system of the machine center. A small point angle twist drill (2) made of K44UF tungsten carbide was employed and its geometric parameters have been listed in Table 2. The selected drilling parameters are 3000 rpm spindle speed, 150 mm/min forward and 500 mm/min backward feed rate. In order to achieve stable temperature data, three holes were drilled on each of the UD and MD CFRP workpieces and the thermal images of the third holes were used for further analyses. All experiments were conducted in dry condition and a dust collector was placed at an appropriate distance to collect only the dust but not the cutting chips. A series of Kistler 9257 B force dynamometer (5), 5080 amplifier, 5697 A data acquisition and force record terminal were employed to measure the cutting force data during the drilling. Original signals of cutting forces were acquired at a sampling frequency of 6 kHz and were processed with a 10 Hz low pass filter. The dynamometer was fixed on the worktable using a T-shape fixture (4), and the CFRP workpiece (3) was inserted in the groove of the fixture and clamped from the drill-entrance side. In addition, the drill is allowed to go through a 16 mm pre-drilled hole on the drill-exit side of the fixture each time to ensure the support stiffness for each drilling hole is consistent. The infrared camera (6) was placed horizontally at the drill-exit side for temperature measurement.

UD and MD CFRP workpieces employed in this work were made from P2352 prepregs with T800S reinforced fiber and 3900-2 B epoxy resin, cured under high temperature and pressure conditions under the manufacturer's specification. The UD CFRP workpiece is 3.1 mm in thickness and consists of 16-layer prepregs in a single orientation. The MD workpiece is 4.3 mm in thickness with 22 layers stacked in different fiber orientations following the sequence $[(-45/0/45/90)_2/0/0/0]_s$. The mechanical properties of UD CFRP composite are summarized in Table 3. The glass transition temperature of the CFRP is about 165C° under dry condition. The ratio of heat conductivities of the material in 0°, 45° and 90° is about 6.7: 4.5: 1 [20]. The fiber cutting angle θ is defined in Fig. 2 based on the view from the drill-exit side.

3. Results and discussion

Fig. 3 illustrates the thrust force variation as a function of the drilling depth and the corresponding frame of the thermal image. The drill-exit surface is defined as the reference plane, and the drilling depth is defined as the distance between the chisel edge and the reference plane. The drilling depth is negative before the drill reaches the drill-exit surface. Five representative positions have been analyzed in detail during the drilling process: Position One (P-I), when the drill chisel edge just reaches the reference plane; Position Two (P-II), when half of the main cutting edge passes the reference plane; Position Three (P-III), when the entire main cutting edge just passes the reference plane;

Table 2
Geometrical parameters of the twist drill.

Diameter (mm)	Point angle (°)	Helix angle (°)	Rake angle (°)	Relief angle (°)	Length of main cutting edge in axial direction of drill (mm)	Length of chisel edge (mm)
8	90	34	15	20	3.63	0.4

Table 3
Mechanical properties of UD CFRP.

Longitudinal tensile strength (MPa)	Transverse compressive strength (MPa)	Longitudinal Young's modulus (GPa)	Transverse Young's modulus (GPa)	Poisson's ration
2842	165.6	160	8.97	0.28

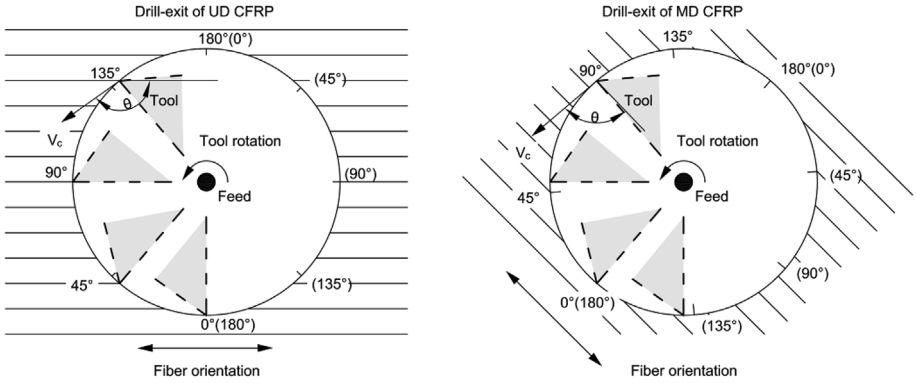

Fig. 2. Definition of fiber cutting angle from drill-exit side in the drilling of UD and MD CFRPs.

Position Four (P-IV), when the minor cutting edge passes the reference plane by 1 mm; and Position Five (P-V), when the minor cutting edge passes the reference plane by 3 mm. Thermal images and the corresponding grey images for the above five positions are listed in Table 4. The dash line represents the calculated real-time diameter of the hole at drill exit (RTD). Drill-exit temperature characteristics of the entire drilling processes have been further investigated through thermal data analyses.

3.1. Temperature characteristics at different drilling depths and the associated drill/CFRP cutting interaction characteristics

3.1.1. Temperature characteristics close to P-I

At P-I, the drill-exit temperature peaked in the hole center and gradually decreased outward, as shown in Table 4 (I). The cutting edge of the drill was not visible in the grey images. This is due to the coverage of the drill-exit material which has been pushed outward and undergone deflection without being penetrated as described in Ref. [26]. The temperature rise at drill exit can be mainly attributed to the heat transferred from the drill and the machined materials. The temperature variations at the drill-exit center can be found in Fig. 4. The temperature was measured from the drill-exit material before it peaked in Fig. 4. It can be seen that the temperatures only start to increase when the chisel edge was about −0.5 mm away from the reference plane. The peak temperature at P-I was about 58.2 °C for UD CFRP and 54.3 °C for MD CFRP. Fig. 3 shows that the thrust force for MD CFRP peaked before the drill reached the reference plane, whereas the thrust force for UD CFRP peaked just after the drill passed the reference plane. This suggested that a stronger constraint was present at the drill-exit in UD CFRP, and as a result, the drill-exit materials were harder to rupture, generating slightly greater cutting heat and higher temperature during drilling. As drilling progressed, the temperatures kept increasing, peaked 105.4 °C in UD CFRP when the chisel edge was about 0.25 mm beyond the reference plane. For MD CFRP, a higher peak temperature (122.5 °C) took place at the similar location, which may be due to the different thickness. Although up to this stage, the temperature maxima was below T_g of the CFRP, it may still lower the strength of the composites in the thickness direction [43,44] which could affect the drilling qualities. As such, it is believed that the existing mathematic models in CFRP machining (e.g., the popular critical thrust force models [3]) could be further refined for better damage prediction and control if the temperature characteristics derived from this study can be taken into account. The temperature began to fluctuate after passing its peak (see Fig. 4). During that period, the temperatures were measured mostly from the drill bit, even though the temperatures of the unremoved materials and the chips at the center of the hole were also likely to be captured.

3.1.2. Temperature characteristics from P-I to P-III

After the chisel edge penetrated the workpiece, most of the drill-exit materials were ruptured along the transverse direction of the outermost layer. The drill-exit materials were cut directly by the main cutting edges resulting in a rapid temperature rise as shown in Table 4(II and III). The highest temperatures in the drilling of UD and MD CFRPs at P-

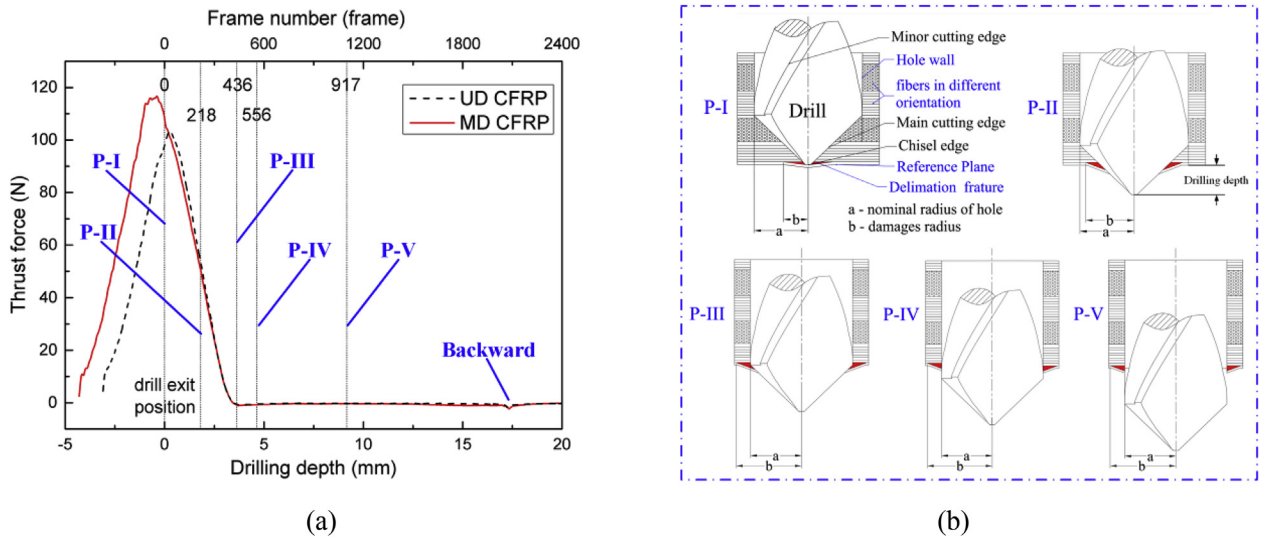

Fig. 3. Thrust force variations (a) thrust force at different drilling depths, (b) schematic diagram of the corresponding drilling positions.

Table 4
Gray and thermal images in different drilling depths (same magnification/scale bar apply to all images).

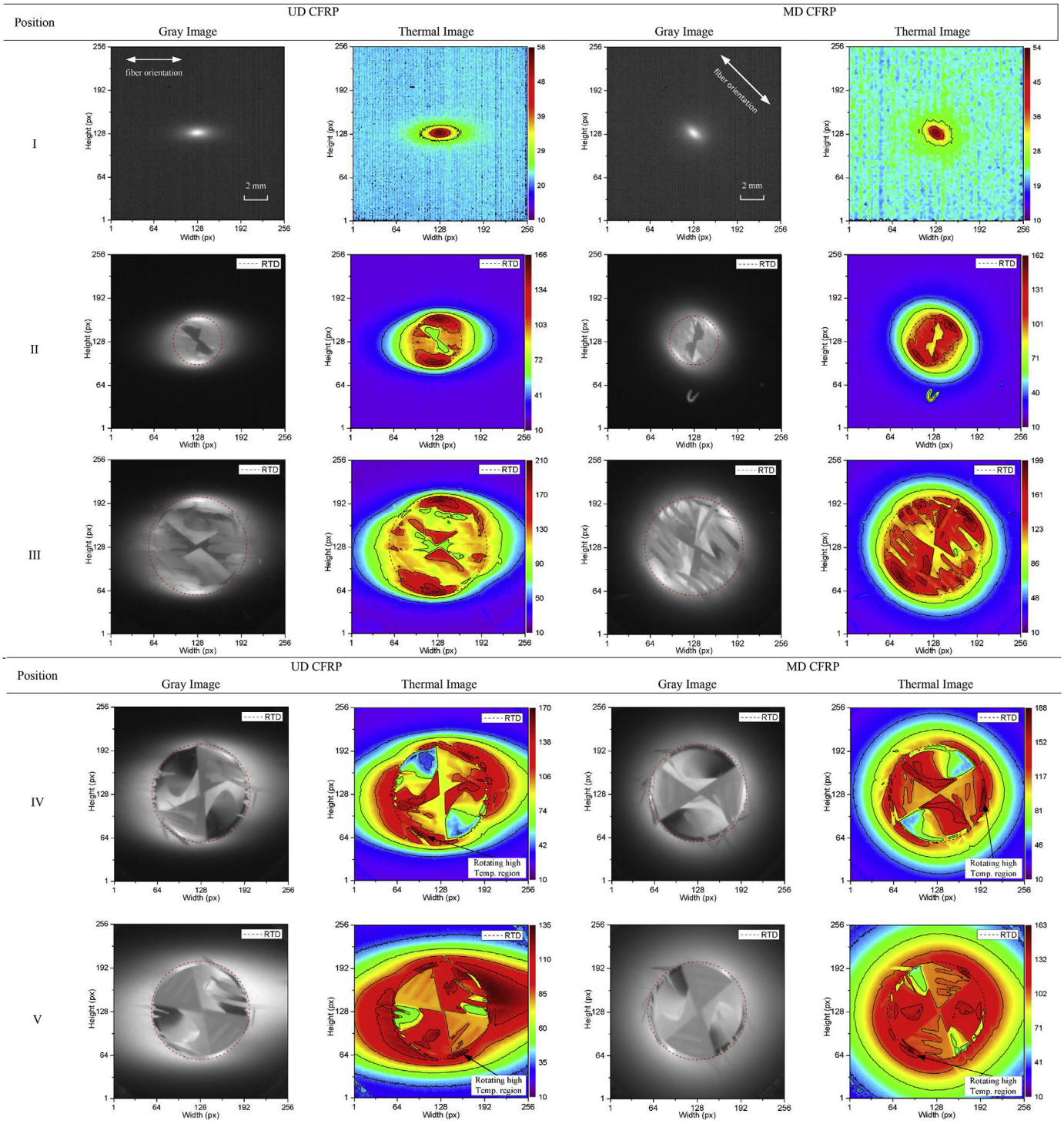

II were above 160 °C, close to T_g of the CFRP. As the hole was being enlarged during drilling, the cutting velocity at RTD increased, leading to more cutting heat that further increased the cutting temperature (up to 210 °C from P-II to P-III). One interesting feature was that in the drilling of UD and MD CFRPs, the high temperature regions both located at $\theta \sim 0°$. This is contradictory to previous reports that the peak temperature was located at $\theta \sim 90°$ [23,24]. The difference could be attributed to that the temperature characteristics were dependent on the measurement method as well as the actual drill/CFRP cutting interactions. In the previous studies [7,9,14,24,36], researchers deployed the thermocouple to measure the temperature from inside of a workpiece. However, as compared to the bulk inner materials, the materials at the drill-exit surface suffered from more severe deflections/damages due to the lack of constraint, therefore different temperature characteristics can be expected. It is believed that the approach proposed in this study is more appropriate for monitoring practical drilling, hence offering a more accurate representation of the temperature characteristics in situ and in real time.

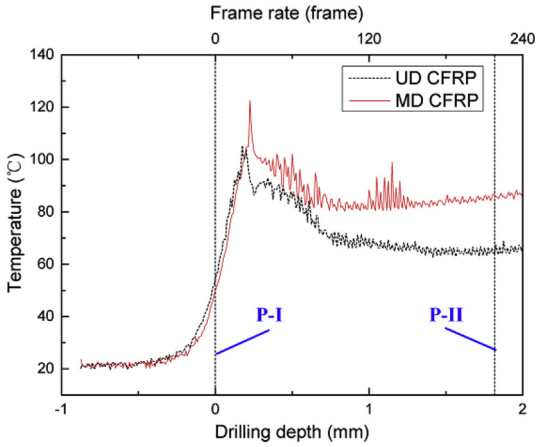

Fig. 4. Temperature variations at the hole center when drill reaches drill-exit area.

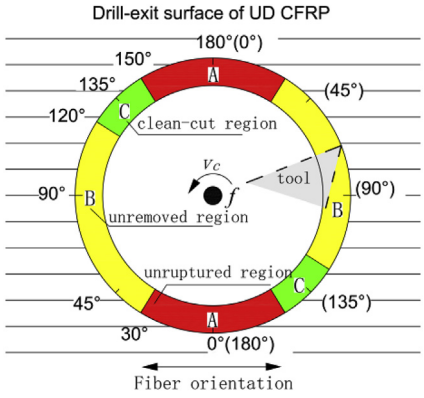

Fig. 6. Partition of drill-exit area based on the actual drill/CFRP cutting interactions (from P-I to P-III).

The actual drill/CFRP cutting interactions at drill-exit have been analyzed in detail to further elucidate the evolution of the temperature difference. The typical cutting processes of UD CFRP have been captured within a half-cycle rotation period and three representative continuous grey images (interval = 0.003 s) are shown in Fig. 5. In Fig. 5(a), the main cutting edge was cutting the materials on the RTD at θ ~ 10°. It can be seen that the materials adjacent to the RTD remained connected and were not ruptured into two parts, as compared to the center materials ruptured from the middle, and hence, the materials adjacent to the RTD were expected to be pushed outwards while being cut. As the main cutting edges advanced to the area at θ ~130°, as illustrated in Fig. 5(b), most of the cutting edges were clearly visible on the RTD, indicating a clean cut of the materials. For the next frame, see Fig. 5(c) θ ~ 70°, the drill-exit materials were hardly removed from the root at the RTD and most of the cutting edges were covered by the unremoved materials, although they were ruptured from the middle. The severe unremoved materials were formed because that in the early drilling period, large initial cracks were generated at drill exit θ ~70° [26] and such cracks will reduce the support of the materials leading to ineffective cut. The cracks were also likely to propagate as the drilling progressed, resulting in larger outward deflections. In addition, more energy is required to remove the materials within that angle range [45] and however, the occurrence of large material deflection makes it more difficult to attain sufficient cutting energy for material removal. The combination of the above factors rendered the cutting action mostly ineffective, leaving a large amount of unremoved materials attached to the cutting edges, see in Fig. 5(c). Similar cutting processes have been found in the drilling of MD CFRP and the details will not be repeated here. With the aid of the in situ thermal images obtained for UD and MD CFRPs, the drill-exit surface could be divided into 3 regions, namely, unruptured region (A, approx. $-30^\circ < \theta < 30^\circ$), unremoved region (B, approx. $30^\circ < \theta < 120^\circ$) and clean-cut region (C, approx. $120^\circ < \theta < 150^\circ$), see Fig. 6.

The above mentioned cutting process continues until P-III was reached, leading to different drill-exit temperature characteristics, see Table 4 (II and III), in each region of Fig. 6. Since the surface materials in the unremoved region (B) were under large outward deflection, experiencing neither severe friction nor effective cutting, less heat was generated, and meanwhile the heat of the inner machined materials could be barely transferred to deflected drill-exit surface. All these factors could contribute to the relatively low temperature in region (B), see in Table 4 (II and III). On the other hand, materials in the unruptured region (A) on the RTD also experienced outward deflection and however, they remained connected, as shown in Fig. 5(a). Therefore, a strong constraint can be expected in the unruptured region and very minor material deflection would take place. The drill-exit materials in region (A) would experience effective cutting from inside associated with severe friction, hence greater heat can be generated. In addition, the drill-exit materials undergoing minor deflection was in close contact with the inner machined materials and could experience more effective heat transfer from the inside. All these would lead to a much greater heat accumulation and temperature rise (even beyond T_g), see the unruptured region in Table 4 (II and III). As a result, it is no longer appropriate to predict the temperature characteristics in practical CFRP drilling only based on the orthogonal cutting results [23] or thermal couple measurement while drilling [24]. In terms of the clean-cut region (C), less heat was accumulated on the drill-exit surface as most materials were removed. Hence the temperature in region (C) was

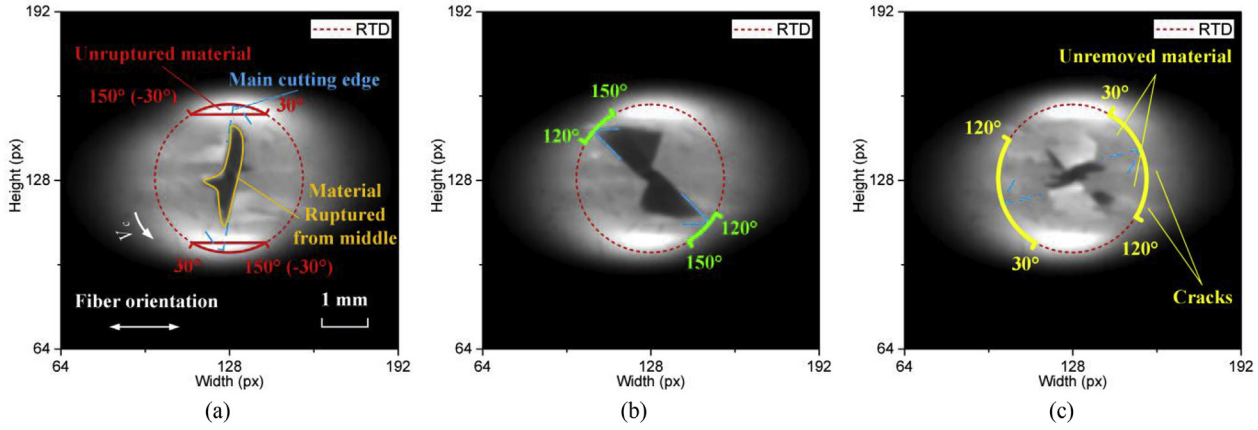

Fig. 5. Three continuous grey images under different fiber cutting angles (UD CFRP, from P-I to P-III) (a) ~10°, (b) ~130°, (c) ~70°.

relatively low, as shown in Table 4 (II and III).

The temperature variations of the inner materials in the present study are in line with the previous literature [23,24], as the inner materials experience less significant deflection. The temperature of the inner materials at θ ~90° was generally higher, leading to a greater reduction of the resin matrix stiffness [43] in that region. This would, in turn, soften the adjacent outer layer, making a clean cut harder to achieve, which could be further validated based on the different drill-exit features seen for UD and MD CFRPs. The areas around θ ~135° in both UD and MD CFRPs were supposed to be in the clean-cut regions. However, the grey images in Table 4 (III) suggested otherwise, i.e., more unremoved materials in MD rather than in UD CFRP. For both UD and MD CFRPs with outermost layer θ ~135°, UD CFPR has all inner layers in the same orientation, whereas for MD CFRP, the longitudinal direction of each inner layer placed 45° clockwise against the next layer outwards. The fiber cutting angle of the layer adjacent to the outermost layer in MD CFRP will be θ ~90°, an angle which would experience higher temperature, rendering a less effective cutting process and a greater amount of unremoved materials at drill exit.

3.1.3. Temperature characteristics after P-III

As drilling progressed from P-III to P-IV and P-V, three distinct temperature characteristics involving minor cutting edges have emerged, as shown in Table 4 (IV and V).

(1) Most of the unremoved materials were gradually cut off from stage P-III to P-IV (see grey images). According to Jia et al. [46], minor cutting edge with the right helical angle was believed to perform upward cutting during downward drilling process with the drill-exit materials being supported from the inner materials of the hole. This in theory facilitates the effective cut of any unremoved materials. However, drills are usually designed with a small helix angle for reasons like chips evacuation, and such geometry would lead to a strong peripheral cutting action, inducing severe Mode II or Mode III cracks and exacerbating the drill-exit splintering [26,47].
(2) Since only unremoved materials were cut off by the minor cutting edge, it would generate less cutting heat after P-III. In the drilling of UD and MD CFRPs, the high temperature region following the end of the rotating main cutting edge can be observed in thermal images in Table 4 (IV and V). The high temperature region corresponded to the contact area between the minor cutting edge and the drill-exit surface, depending on the local drilling depth and tool geometry, and the heat was predominantly generated by friction.
(3) In contrast to P-III, the high temperature regions of P-IV and P-V have shifted to θ ~ 90° for UD CFRP, with the frictional heat dominating over the cutting heat. There are mainly two factors contributing to the temperature shift. (i) Materials at θ ~ 0° were located in the unruptured region prior to P-III and were mostly removed after P-III. This resulted in little accumulated heat in that region. (ii) Fiber cutting angles have a different influence on the frictional heat and the cutting heat generated. Friction and the frictional heat are closely related to the normal stress and the frictional coefficient between the minor cutting edge and the machined surface. The normal stress increases with increasing relative height of the machined hole wall. In order to reveal the relationship between frictional heat and fiber cutting angles, the machined hole wall of MD CFRP has been analyzed.

The machined hole wall of MD CFRP has been divided into three sections along its peripheral direction. Fig. 7(a) shows laser confocal images (laser confocal microscopy VK-X1000, Keyence) of selected positions (colored lines) on different sections across layers under 0°, 45°, 90° and 135° fiber cutting angle. The average height of the selected positions was measured along the color lines, and only the middle section of the selected area was analyzed to rule out the influence of unstable drilling generated at exit [10]. A lower height can be seen in all three positions at θ ~135° in Fig. 7(b), this was consistent with the concave dent features commonly seen in this region [48]. The lower height could be attributed to the severe subsurface damage at that angle which has been fundamentally studied in Ref. [49]. As a result, materials in this region were not touching the cutting tool or being rubbed under a small normal stress hence leading to little friction and frictional heat. The relative heights for the three positions were similar for 0° < θ < 90°. However, since the frictional coefficient is expected to increase from 0° to 90° [50], a greater frictional heating and a higher temperature should be expected for θ ~ 90°. This explains the shift of the high temperature region to θ ~90° in P-III to P-IV for UD CFRP under friction dominated heating. However, no obvious temperature shift has been found for drilling of MD CFRP, and this can be attributed to the quasi-isotropic lay-up sequence of the composite, leading to a more uniform heat distribution in all directions.

3.2. Temperature distributions

Table 4 illustrates the drill-exit temperature distributions at five different locations in the drilling of UD and MD CFRPs. For both composites, most temperature isotherms featured elliptical shapes, the centers of which corresponded to the hole centers and the major and minor axes corresponded to the longitudinal and the transverse directions of the outermost layer at drill exit respectively. In cutting of CFRP, more cutting and frictional heat has been generated at θ ~90° [23], except for the outermost layer. The heat would conduct more quickly to the remote area along the longitudinal direction due to its higher thermal conductivity [51]. As a result, the temperature rise in the more remote area was expected, resulting in the elliptical temperature isotherm.

In order to make a quantitative analysis, the temperature isotherms of 40 °C and 50 °C in each thermal image have been selected to describe the temperature distribution, as they suffered less from fiber deflections. The eccentricities of the temperature distribution ellipses were calculated, and the results were shown in Fig. 8. The eccentricities in UD CFRP were distinctively higher than those in MD CFRP. This could again be explained by the difference in heat conduction in composites with the different lay-up sequences. In UD CFRP, the main heat transfer was along the fiber direction throughout the material, therefore the heat accumulation and the subsequent temperature rise in the remote area at the exit surface also followed the same trend, i.e. a high-eccentricity ellipse. However, in MD CFRP the main heat transfer paths in adjacent layers were 45° apart. Under such circumstances, the high temperature region of one layer was in direct contact with the low temperature region of the adjacent layer. This anisotropic structure gradually compensated the anisotropic heat conduction as the drill went through the material, and therefore a more circular temperature isotherm was obtained.

On the other hand, the variations of the eccentricity at different drilling depths in Fig. 8 show different trends for UD and MD CFRPs. Specifically, the eccentricity in MD CFRP dropped rapidly from P-I to P-V, with the shape of the temperature isotherm gradually approaching a circle. In contrast, the eccentricity in UD CFRP only slightly declined from P-I to P-III and increased from P-IV to P-V. The initial decrease of the eccentricity in both composites may be because much heat has been accumulated at θ ~0°, close to the direction of the minor axis of the ellipse. However, the steady state has been disrupted when the frictional heating dominates after P-III, as explained in Section 3.1. Hence with the drill-exit materials at θ ~0° being removed, more frictional heat has been generated on the drill-exit surface at θ ~90°. This again promoted the anisotropic heat transfer and increases the eccentricity of the temperature distribution in UD CFRP.

3.3. Real-time temperature on the normal diameter

The temperature on the normal diameter of the hole at drill exit is

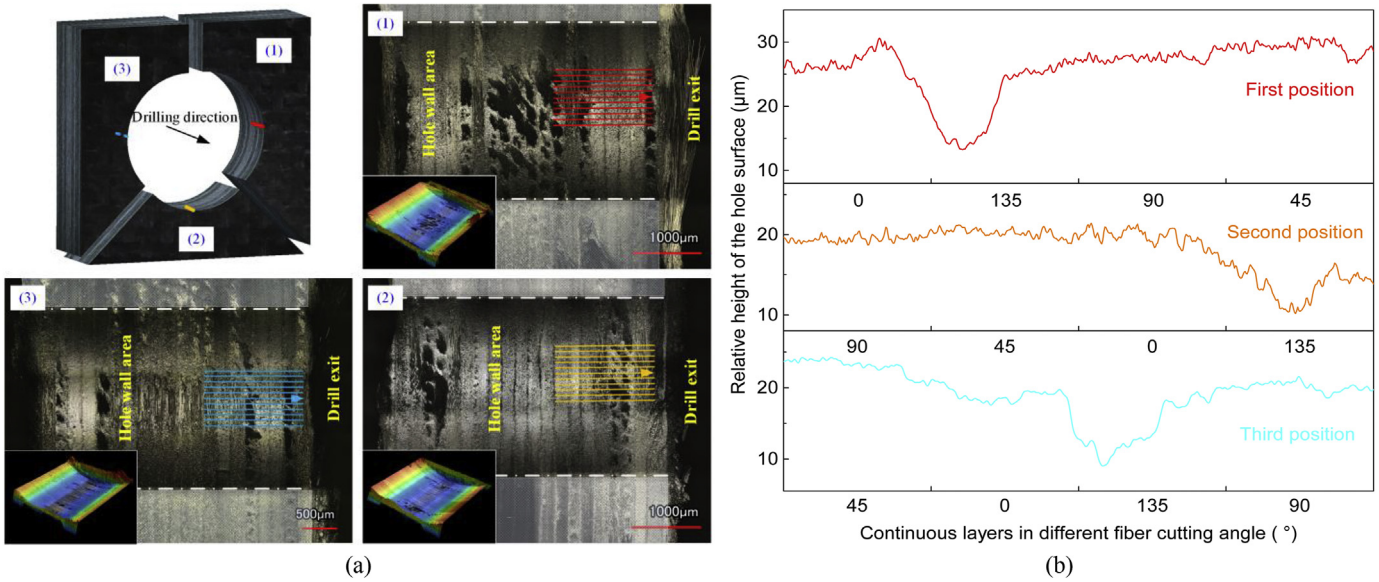

Fig. 7. Machined hole wall features (a) optical images, (b) average heights of three positions.

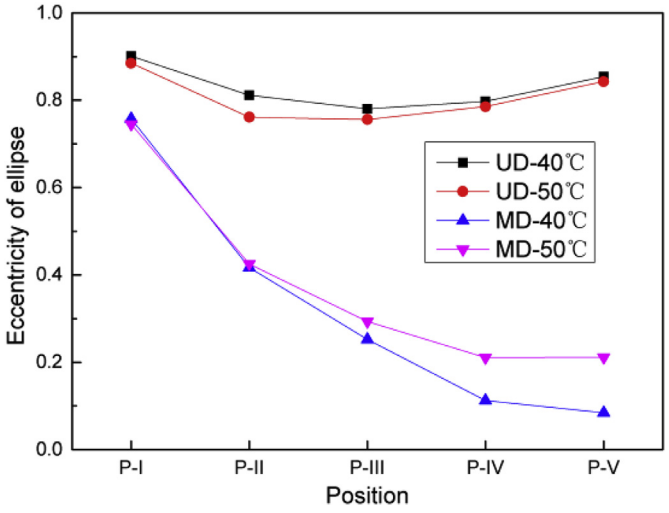

Fig. 8. Variations of eccentricity at different positions.

key to determine the heat affected zones in the drilling of CFRP. Those temperature data were obtained through post processing a circle edge with a radius of two pixels larger than the actual hole radius from the thermal images. The real-time temperatures on the normal diameter in the drilling of UD and MD CFRPs were visualized as shown in Fig. 9 with the temperature threshold for each position labeled. Before P-II, half of the drill penetrated the exit, the temperatures on the normal diameter were below 40 °C for both composites. When the drill reached P-III, the high temperature region in UD CFRP changed from θ ~90°–~22.5°, see the direction of the white arrow in Fig. 9 (a) and the temperature maxima approached about 126 °C. In contrast, almost no change of high temperature region has been observed for MD CFRP with temperature maxima only approaching about 102 °C at θ ~0°. The ultimate maximum temperatures on the normal diameter (~156 °C for UD CFRP and ~163 °C for MD CFRP), emerged in the similar angle range and between P-III and P-IV. However, they were much lower than the temperatures within the normal diameter measured during the same period as shown in Table 4. The heat affected zone in the drilling of CFRP was defined as the area where the temperature exceeds T_g [20]. However, the measured maximum temperature indicated that no heat affected zone has formed in this study, and the drilling qualities should be barely affected by high temperature. However, as a matter of fact, the temperature characteristics measured by the thermal imaging system were determined by the actual drill/CFRP cutting interactions as described in Section 3.1. Justification of the temperature effects on drilling qualities solely based on the measured temperature characteristics is not sufficient. Therefore, further investigation on the actual temperature effects has been carried out in conjunction with the drill-exit layer micro-topography analysis.

As it can be seen from Fig. 9, temperatures rose rapidly from P-II to P-III. The average temperature increase rate, v_T, in a particular fiber cutting angle has been defined as,

$$v_T = \frac{T_M - T_I}{t} \quad (1)$$

where T_M is the temperature measured at a particular point of time during drilling, T_I is the temperature measured at the start of drilling and t is the time difference. v_T for $T_M = 40$ °C and $T_M = 70$ °C were calculated for the area from 0° to 180° fiber cutting angle, see Fig. 10. As the drilling progressed, v_T increased rapidly. For UD CFRP at 40 °C, v_T at θ ~90° was about 1.7 times greater than that at θ ~0°, and for UD CFRP at 70 °C, 1.4 times greater. For MD CFRP, on the other hand, v_T experienced minor variation across the whole angle range. Within the regions approx. 0° < θ < 45° and approx. 120° < θ < 180°, v_T was even higher than those with the same angles in UD CFRP.

3.4. Maximum temperatures at drill exit

The maximum temperature of every single pixel in all the thermal images were obtained through high volume thermal data processing. Three-dimensional (3D) distribution maps of the maximum temperatures were created for the first time, visualizing/describing the whole drilling process of UD and MD CFRPs, see Fig. 12 (a) and (b), with the temperature thresholds between each position labeled. Both 3D distribution maps could be divided into two parts according to the drilling depth and the normal diameter of the hole: (i) before the main cutting edges completely penetrated at P-III, and (ii) after P-III. For part (i), cutting heat and frictional heat, etc. were concentrated within the normal diameter and the temperature of most area within the normal diameter reached the highest value, see in Fig. 11. From the 3D distribution maps, it was difficult to determine whether the maximum temperatures were from the machined workpiece, the drill or the chips. For part (ii), Fig. 11 suggests that maximum temperatures of the area

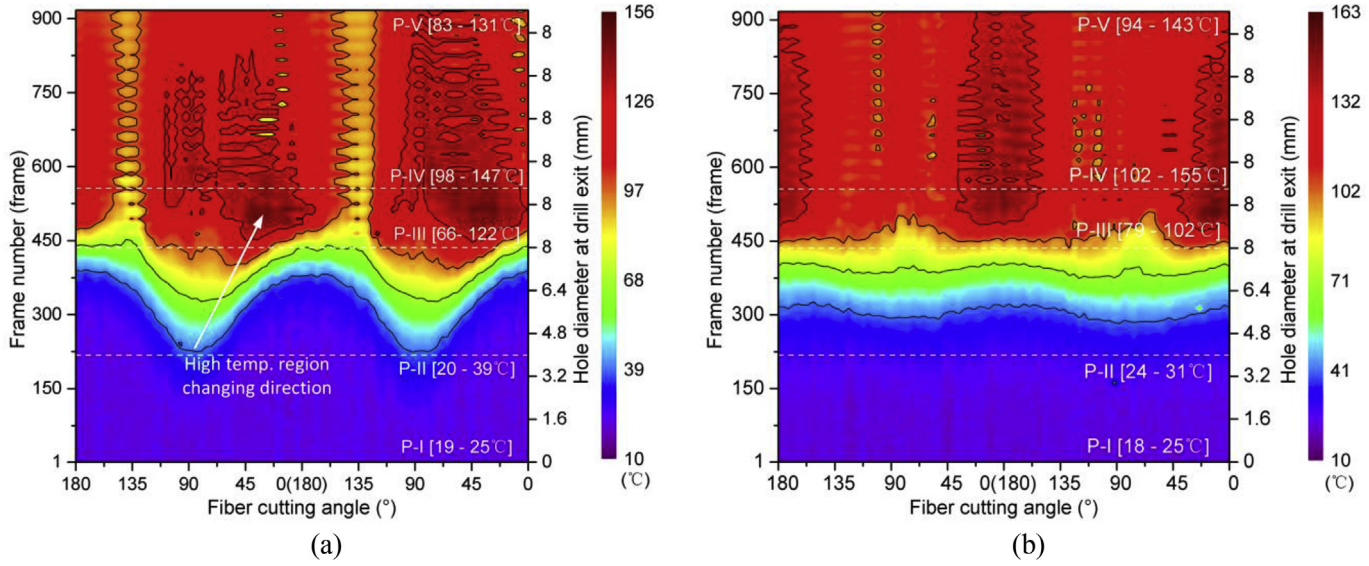

Fig. 9. Real-time temperature on the normal diameter of the hole on the drill-exit surface (white text illustrates the temperature thresholds for each position) (a) UD CFRP, (b) MD CFRP.

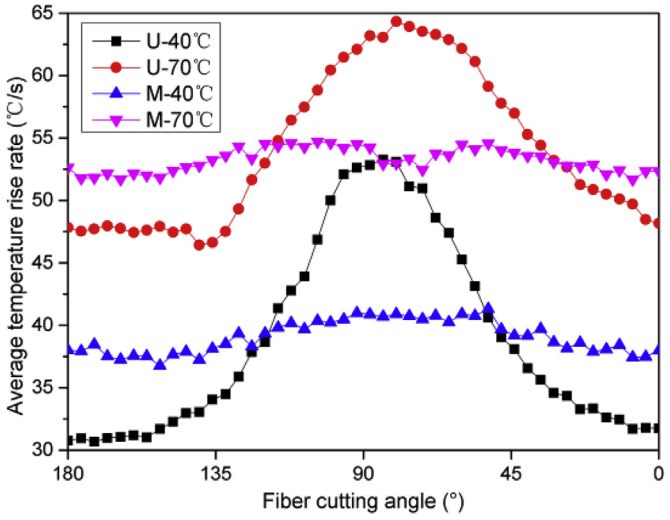

Fig. 10. Average temperature increasing rate approaching 40 °C and 70 °C.

outside the normal diameter were generally achieved. In this region, most of the maximum temperatures were measured from the machined workpiece as only a few chips were extracted from the exit through the right-hand helix flute of the drill. Therefore, in addition to the temperature rise induced by the cutting action of main cutting edges, the drill-exit temperatures outside the normal diameter increased again under the cutting action of minor cutting edges. The secondary temperature rise might potentially affect the hole qualities and hence the feeding distance should be carefully controlled to avoid a long cutting period involving minor cutting edges in drilling of CFRP.

The 3D distribution maps in Fig. 11 were reconstructed into two-dimensional planar (2D) planar distribution maps as shown in Fig. 12(a) and (b), with the origin located at the hole center. The areas with maximum temperatures greater than T_g, have been marked by solid isotherm lines. It can be seen that such areas are located in the region approx. $-25^\circ < \theta < 25^\circ$, for both UD and MD CFRP. In contrast, maximum temperatures of the area outside the normal diameter rarely exceeded T_g. As described in Section 2.2, the emissivity of the thermal imaging system has been adjusted for CFRP temperature measurement. As a result, the emissivity value was much greater than what was required for drill materials, hence the temperature measured

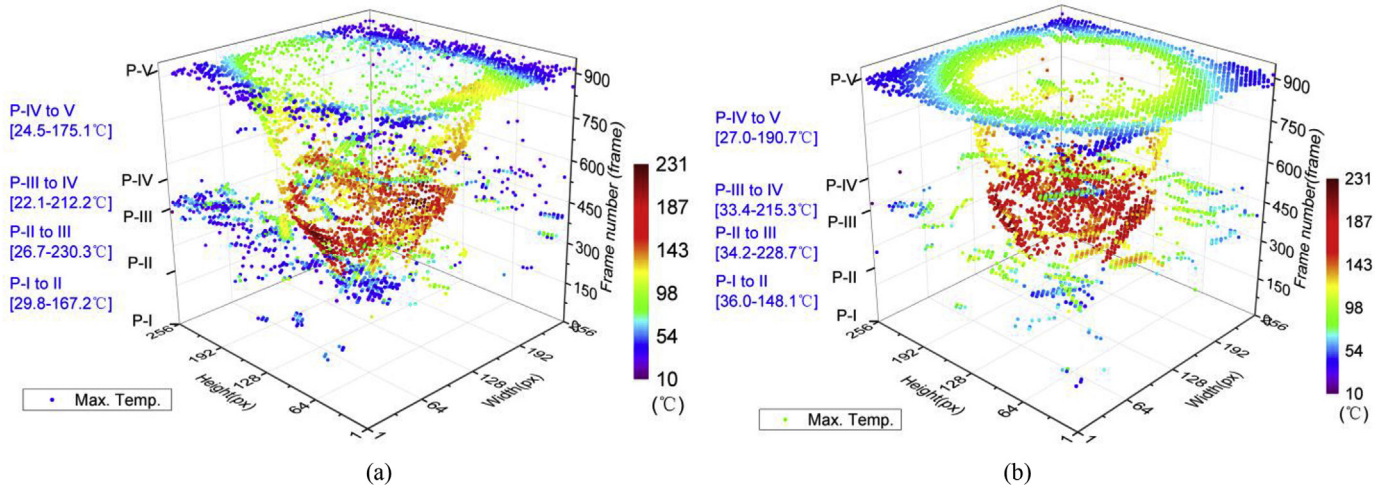

Fig. 11. Three-dimensional distribution maps of maximum temperatures at drill-exit surface (blue text illustrates the temperature thresholds between each position) (a) UD CFRP (b) MD CFRP. (For interpretation of the references to color in this figure legend, the reader is referred to the Web version of this article.)

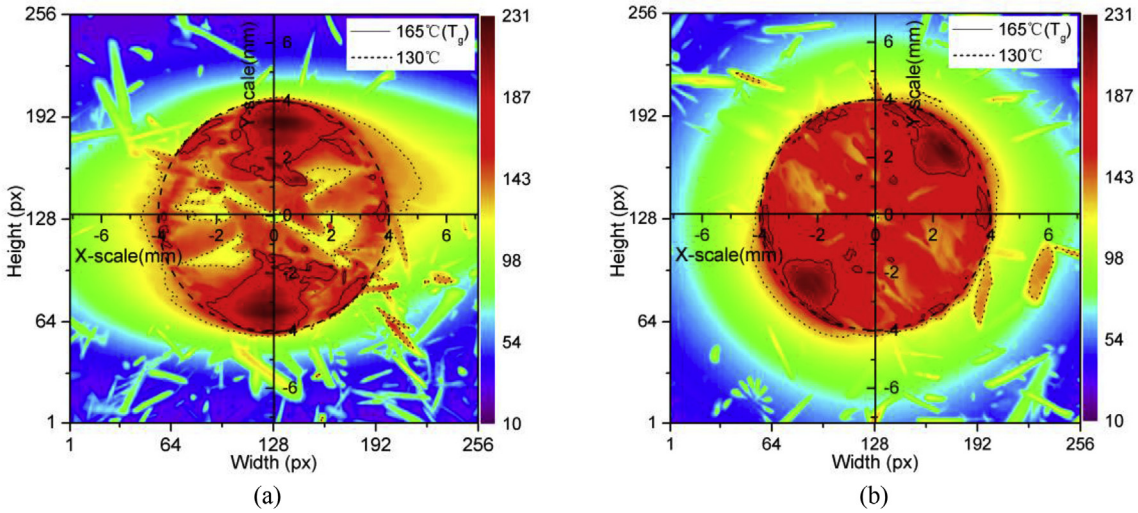

Fig. 12. Two-dimensional planar distribution maps of maximum temperatures at drill-exit surface (a) UD CFRP, (b) MD CFRP.

for the drill can be significantly underestimated [52]. Meanwhile, combining results from the drills and the workpieces from Table 4(III), it can be concluded that the maximum temperature area in Fig. 12 (marked by solid isotherm line) is not from the drill. Additionally, the measured temperature of chips (mostly in short strips) in Fig. 12 should be lower than that of the materials being cut within the normal diameter. Therefore, it is believed that the marked areas with the maximum temperature values above T_g were CFRP workpiece.

The highest drill-exit temperatures for UD and MD CFRPs were both confirmed to be ~231 °C during the whole drilling process even though the material thicknesses were slightly different. As shown in Fig. 12, the highest temperatures did not appear on the normal diameter position where the cutting speed reached the highest value, even though the temperature of the cutting area would rise with the increasing cutting speed [53,54]. Instead, they were located within the area ~0.5 mm inside the normal diameter. This has reflected the close relationship between the temperature characteristic and drill/CFRP interactions: (i) with the hole being enlarged, most materials have been removed, and hence less heat was generated as compared to the earlier cutting period. The heat transferred from the uncut materials to the drill-exit surface would also reduce correspondingly. (ii) before the main cutting edge completed its final cutting action, only a few uncut materials remained at the drill-exit surface which consequently were in a low stiffness condition. In addition, the real-time temperature in the region next to the normal diameter has already exceeded T_g. This could further lower the stiffness of the uncut materials. Due to the decreased stiffness, the materials on the normal diameter could not be cut effectively and hence less cutting heat was generated. As a result, the highest temperature on the normal diameter was lower than that of the inside region. Given the maximum temperature characteristics above, more effective cooling strategies can be proposed, for instance, the location of the cooling hole on drills could be optimized to achieve a better control of the temperature in the drilling of CFRP.

Furthermore, for the area outside the normal diameter, it was found that the high temperature regions (> 130 °C) in the drilling of UD CFRP were located within approx. $10^\circ < \theta < 115^\circ$ (marked by dot isotherm line). This region has extended to ~1 mm outside the normal diameter, as shown in Fig. 12(a), where severe debonding was clearly evidenced, see Table 4. In comparison, the high temperature regions in the drilling of MD CFRP were located within approx. $-30^\circ < \theta < 30^\circ$ and extended ~0.5 mm outside the normal diameter, see Fig. 12(b).

The above finding suggests that the technology of this paper could be generalized and further utilized in investigating temperature characteristics of other materials. Especially for composites like ceramic matrix composite with similar material structure [55], high qualities of the temperature features could probably be obtained under proper measuring parameters and similar post-processing progress.

3.5. Temperature effects on hole qualities

The high temperature induced by the drilling process is expected to have an impact on the quality of the drilled holes. However, little information regarding drilling quality could be revealed only through the thermal image analysis. Therefore, the microstructures on the hole walls in proximity to the drill-exit surface have been further studied. Fig. 13 shows the typical SEM images of the drill-exit hole wall within approx. $-30^\circ < \theta < 30^\circ$. Damages like burrs, debonding and fiber pull-out were all located in the outermost layer of UD and MD CFRPs and featured differently for specific fiber cutting angles. Based on the observation, the damages in the drilling of MD CFRP were more severe. Referring to the outermost layer at $\theta \sim 30^\circ$, the width of the relative smooth surface in MD CFRP (57.51 μm) was much smaller than that in UD CFRP (101.57 μm). Meanwhile, at $\theta \sim -30^\circ$, severe fiber pull-out and debonding in MD CFRP were found as compared to UD CFRP. Due to that the thrust forces induced by the drill bit at the end of the drilling process were similar for UD and MD CFRPs according to Fig. 3, the damage differences could be attributed to the unique force and/or thermal interactions between the outermost and inner layers induced by the distinct lay-up sequences of UD and MD CFRPs. The interlaminar force between the outermost and inner layers needs a direct contact medium to be transferred and affect the outermost layer. However, based on the observation in Fig. 13, the damages were only within the outmost layer and did not expand to the inner layers. This suggests that the interlaminar force did not cause strong interactions between the outmost and inner layers and affect the damage differences and hence, the effects of the interacting force between the outermost and inner layers can be neglected. In contrast, the thermal interaction could affect the cutting without direct contact between the outermost and inner layers due to the presence of temperature field. Therefore, the temperature effects are predominant for the damage differences between UD CFRP and MD CFRP. As shown in Fig. 12, the regions within approx. $-30^\circ < \theta < 30^\circ$ slightly outside the normal diameter were under high temperature for MD CFRP only, where a greater degree of damages in MD CFRP were observed, verifying the temperature effects on drilling qualities.

Fig. 14 shows the drill-exit surfaces of UD and MD CFRPs captured by the laser scanning confocal microscope (VK-X1000, Keyence) under a deep-scan function. Results show that most drilling damages

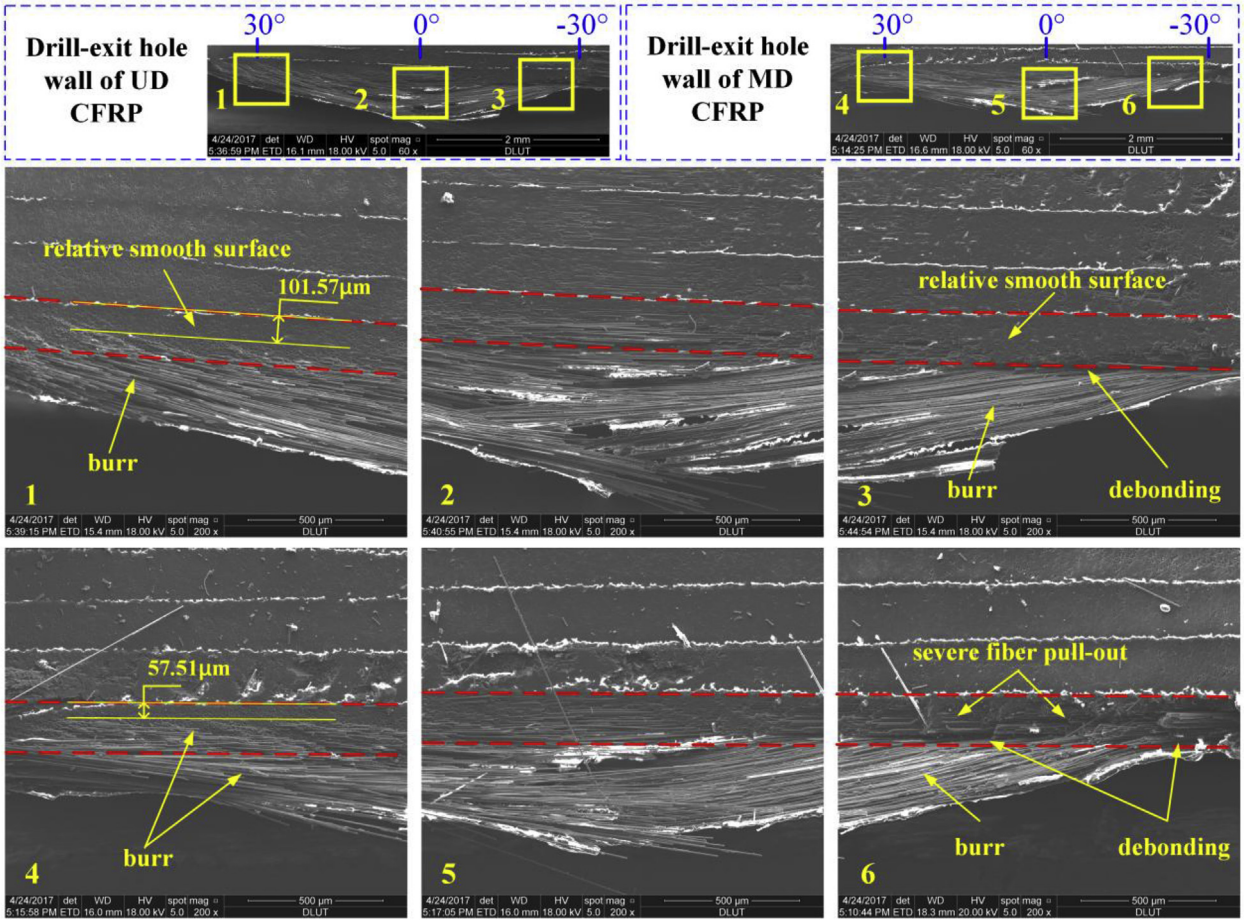

Fig. 13. Microstructures of machined hole wall within region approx. $-30^{\circ} < \theta < 30^{\circ}$ at a representative drill exit (the area between the two red dash line is the outermost layer at drill exit). (For interpretation of the references to color in this figure legend, the reader is referred to the Web version of this article.)

(including burrs and splintering) appeared in areas at similar fiber cutting angles, even though the drill-exit temperature characteristics were distinctly different for UD and MD CFRPs. In both cases, most burrs were found at $\theta \sim 45^{\circ}$, and the fibers at $\theta \sim 90^{\circ}$ were more likely to be torn. However, the splintering of MD CFRP occurred over a larger area (up to $\theta \sim 144^{\circ}$), see Fig. 14(b), whereas for UD CFRP, the splintering did not go beyond 122°, as shown in Fig. 14(a). The maximum angles of splintering area for six holes (3 for each type of CFRP) have been measured and listed in Table 5, and results suggested that MD CFRP was more likely to experience splintering in the large angle area.

Table 5
Maximum fiber cutting angles of splintering areas.

Hole Number	1	2	3
UD CFRP	114.44°	123.20°	121.47°
MD CFRP	144.04°	143.64°	144.59°

The microstructures of the drill-exit hole walls at $\theta \sim 135^{\circ}$ (between 122° and 144°), see Fig. 15, have been studied to further elucidate the damage mechanisms within the large angle region of UD and MD

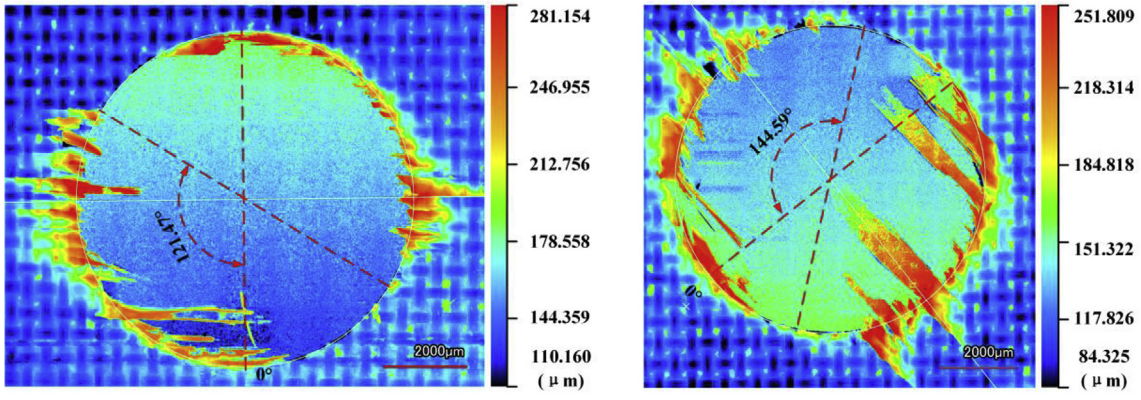

(a) (b)

Fig. 14. Drill-exit surface (a) UD CFRP, (b) MD CFRP.

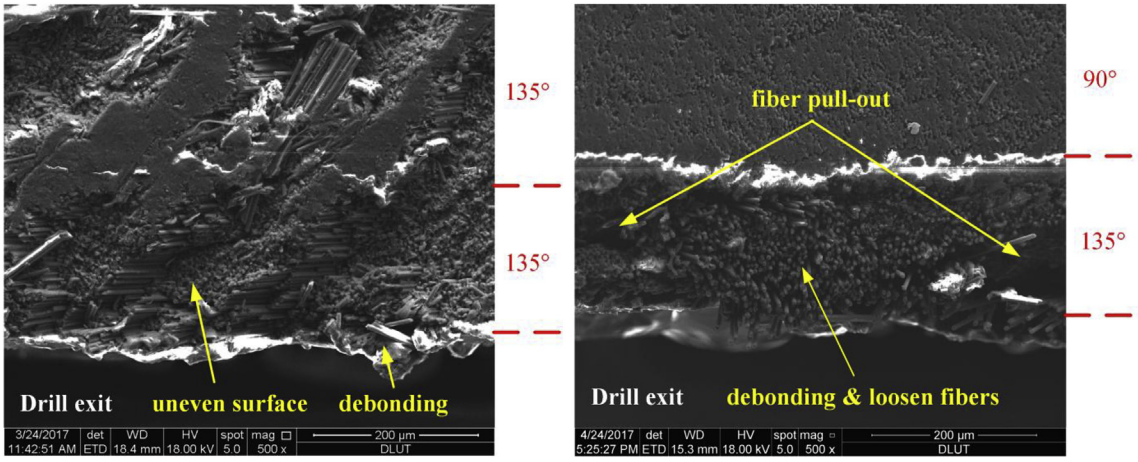

(a) (b)

Fig. 15. Microstructures of the machined hole wall at θ ~135° at drill exit (a) UD CFRP, (b) MD CFRP.

CFRPs. Fig. 15(a) illustrated that the materials within the outermost layer in the drilling of UD CFRP were cut off directly, leaving the typical uneven surface [56] and few debonding damages. In contrast, many fiber pull-out and debonding damages can be found in the outermost layer in the drilling of MD CFRP within the same angle region, as shown in Fig. 15(b). Similar to the damage analyses of Fig. 13 above, the damages within the large angle region in Fig. 15 have been constrained to the outermost layer, and the effects of the interacting force between the outermost and inner layers can be neglected. Then, the temperature effects were expected to play an important role for the damage differences between UD CFRP and MD CFRP due to the presence of the temperature field. However, it was difficult to be verified from the thermal images as some serious debonding at θ ~135° may affect the temperature comparison. Even so, the temperature effects could still be evaluated by the temperature variations with fiber cutting angles and lay-up sequences. The inner layers adjacent to the outermost layer at θ ~135° were at θ ~135° for UD CFRP and at θ ~90° for MD CFRP. Similar to the discussions in Section 3.1, higher temperatures of the inner layer were expected for θ ~90°. This would lead to more severe material softening and bonding strength reduction of the outermost layer θ ~135° in the drilling of MD CFRP. Consequently, a greater amount of fiber pull-out and debonding damages were observed within the large angle region of MD CFRP.

4. Conclusions

Temperature is a key factor in the drilling of CFRP and this paper has thoroughly investigated drill-exit temperature characteristics in the drilling of UD and MD CFRPs through the advanced infrared thermography technology. The following conclusions have been reached:

1. The actual drill/CFRP cutting interactions in UD and MD CFRPs have critical but similar effects on the drill-exit temperatures. When the chisel edge penetrates CFRP, temperature maxima occur at the hole center but is relatively low as the chisel edge mainly pushes CFRP without effective cutting. As the main cutting edges start cutting the drill exit materials, different temperature characteristics emerged in three distinct cutting regions. Unruptured region (approx. $-30^\circ < \theta < 30^\circ$) features higher temperature, as the unruptured materials work against deflection, which results in effective cutting, heat transfer as well as severe friction, and hence much heat is accumulated. Unremoved region (approx. $30^\circ < \theta < 120^\circ$) features lower temperature because the materials are under large deflection leading to ineffective cutting and heat transformation. For clean-cut region (approx. $120^\circ < \theta < 150^\circ$), heat is barely accumulated at drill exit as most materials are removed, resulting in a lower temperature. When the minor cutting edges are acting on drill exit, high temperature regions shift from approx. 0°–90° in UD CFRP. This can be correlated to the varied machined hole wall profiles and the associated frictional coefficients.
2. The real-time temperature profiles and 2D/3D maximum temperature distribution maps are created with high visualization. Almost all areas with temperatures beyond T_g are within the normal diameter, and the peak temperatures in this region are found before the drill exit materials being cut by minor cutting edges. For UD and MD CFRPs respectively, the temperature maxima (up to 231 °C) in the entire drilling process are neither located at the hole center (105.4 °C and 122.5 °C) nor on the normal diameter (156 °C and 163 °C) but within the area ~0.5 mm inside the normal diameter in the region approx. $-25^\circ < \theta < 25^\circ$. Besides, most areas outside the normal diameter encounter a secondary temperature rise when the minor cutting edges acting on the drill exit, which might potentially affect hole qualities.
3. Temperature distributions at the UD and MD CFRPs drill exits feature the elliptical shape. The eccentricity of the ellipse varies with lay-up sequence and drilling depths. Eccentricities in MD CFRP are much smaller and only show a declining trend. However, besides the decreasing trend, eccentricities in UD CFRP change to increase during minor cutting edges acting because the cutting interaction changes promote the anisotropic heat transfer.
4. Temperature characteristics have strong effects on the actual drill/CFRP cutting interactions and the resulting drilling qualities. Due to the temperature effects, the damages observed in the drilling of MD CFRP are more severe. The high temperature within region approx. $-30^\circ < \theta < 30^\circ$ results in a reduction of the smooth surface at θ ~30° and leads to more severe fiber pull-out and debonding at θ ~ −30° on the outermost layer. Splintering frequently occurs on the outermost layer within large angles in MD CFRP (approx. from 122° to 144°), coinciding with the different temperature effects induced by the distinct lay-up sequences of the workpieces.
5. This study has provided important findings, which can help refine the existing theoretical and simulation models in CFPR drilling. It has also offered new perspectives that could inform future strategies in the optimization of the CFRP drilling process, as well as improvements of the material and cutting tool designs.

Acknowledgements

This work is supported by National Natural Science Foundation of China-United with Liaoning Province (No. U1508207), National

Natural Science Foundation of China (No. 51575082), National Key Basic Research Program of China (973 Program, No. 2014CB046503), National Innovative Research Group (No. 51321004), Fundamental Research Funds for the Central Universities (No. DUT16TD01), UK EPSRC projects EP/P025447/1 and EP/P026087/1, and EU H2020 RISE 2016 - ECSASDPE 734272 project.

References

[1] US Department of Energy, Advanced composites materials and their manufacture technology assessment, Quadrenn. Technol. Rev. (2015) 1–37 https://www.energy.gov/sites/prod/files/2015/02/f19/QTR%20Ch8%20-%20Composite%20Materials%20and%20Manufacture%20Feb-13-2015.pdf , Accessed date: 28 June 2018.
[2] G. Sala, Composite degradation due to fluid absorption, Compos. B Eng. 31 (2000) 357–373.
[3] U.A. Khashaba, Drilling of polymer matrix composites: a review, J. Compos. Mater. 47 (2013) 1817–1832.
[4] K. Weinert, C. Kempmann, Cutting temperatures and their effects on the machining behaviour in drilling reinforced plastic composites, Adv. Eng. Mater. 6 (2004) 684–689.
[5] F. Ning, H. Wang, W. Cong, P.K.S.C. Fernando, A mechanistic ultrasonic vibration amplitude model during rotary ultrasonic machining of CFRP composites, Ultrasonics 76 (2017) 44–51.
[6] W. Chen, Some experimental investigations in the drilling of carbon fiber-reinforced plastic (CFRP) composite laminates, Int. J. Mach. Tool Manufact. 37 (1997) 1097–1108.
[7] C. Ramirez, G. Poulachon, F. Rossi, R. M'Saoubi, Tool wear monitoring and hole surface quality during CFRP drilling, Proc. CIRP 13 (2014) 163–168.
[8] J.L. Merino Pérez, R. Royer, E. Merson, A. Lockwood, S. Ayvar-Soberanis, M.B. Marshall, Influence of workpiece constituents and cutting speed on the cutting forces developed in the conventional drilling of CFRP composites, Compos. Struct. 140 (2016) 621–629.
[9] Z. Jia, R. Fu, F. Wang, B. Qian, C. He, Temperature effects in end milling carbon fiber reinforced polymer composites, Polym. Compos. 39 (2018) 437–447.
[10] J.L. Merino Pérez, A. Hodzic, E. Merson, S. Ayvar-Soberanis, Induced thermo-mechanical damage in the drilling of thermoplastic-toughened CFRP composites, Proceedings of the 20th International Conference on Composite Materials ICCM-20, Copenhagen, Denmark, July 19-24, 2015.
[11] J.L. Merino Pérez, A. Hodzic, S. Ayvar, E. Merson, The influence of heat during short ageing periods on the mechanical properties of CFRP composites, Proceedings of 16th European Conference on Composite Materials ECCM-16, Seville, Spain, June 22-26, 2014.
[12] J.L. Merino Pérez, A. Hodzic, S. Ayvar-Soberanis, E. Merson, S. Ayvar-Soberanis, On the temperatures developed in CFRP drilling using uncoated WC-Co tools Part II: nanomechanical study of thermally aged CFRP composites, Compos. Struct. 123 (2015) 30–34.
[13] A. Chatterjee, Thermal degradation analysis of thermoset resins, J. Appl. Polym. Sci. 114 (2009) 1417–1425.
[14] W. Ben, G. Hang, W. Quan, W. Maoqing, Z. Songpeng, Influence of cutting heat on quality of drilling of carbon/epoxy composites, Mater. Manuf. Process. 27 (2012) 968–972.
[15] E. Persson, I. Eriksson, L. Zackrisson, Effects of hole machining defects on strength and fatigue life of composite laminates, Compos. Part a Appl. Sci. Manuf. 28 (1997) 141–151.
[16] Y. Turki, M. Habak, R. Velasco, Z. Aboura, K. Khellil, P. Vantomme, Experimental investigation of drilling damage and stitching effects on the mechanical behavior of carbon/epoxy composites, Int. J. Mach. Tool Manufact. 87 (2014) 61–72.
[17] A. Abdel Hamid, A.S. Wifi, M. El Gallab, A three dimensional finite element thermomechanical analysis of intermittent cutting process, J. Mater. Process. Technol. 54 (1996) 643–654.
[18] M. Bacci da Silva, J. Wallbank, Cutting temperature: prediction and measurement methods—a review, J. Mater. Process. Technol. 88 (1999) 195–202.
[19] M.A. Davies, T. Ueda, R. M'Saoubi, B. Mullany, A.L. Cooke, On the measurement of temperature in material removal processes, CIRP Ann. Manuf. Technol. 56 (2007) 581–604.
[20] C.T. Pan, H. Hocheng, Evaluation of anisotropic thermal conductivity for unidirectional FRP in laser machining, Compos. Part a Appl. Sci. Manuf. 32 (2001) 1657–1667.
[21] T. Tian, K.D. Cole, Anisotropic thermal conductivity measurement of carbon-fiber/epoxy composite materials, Int. J. Heat Mass Tran. 55 (2012) 6530–6537.
[22] F. Wang, J. Liu, Y. Liu, Y. Wang, Research on the fiber lay-up orientation detection of unidirectional CFRP laminates composite using thermal-wave radar imaging, NDT E Int. 84 (2016) 54–66.
[23] S. Qin, Z.W. Li, H.Z. Zhang, Q.L. An, M. Chen, Experimental study on orthogonal cutting of 0° T700/LT03A CFRP uniform laminates, Mater. Sci. Forum 800–801 (2014) 76–80.
[24] W. Hintze, C. Schütte, S. Steinbach, Influence of the fiber cutting angle on work piece temperature in drilling of unidirectional CFRP, New Prod. Technol. Aerosp. Ind. Springer, 2014, pp. 137–143.
[25] J. Liu, G. Chen, C. Ji, X. Qin, H. Li, C. Ren, An investigation of workpiece temperature variation of helical milling for carbon fiber reinforced plastics (CFRP), Int. J. Mach. Tool Manufact. 86 (2014) 89–103.
[26] G. DiPaolo, S.G. Kapoor, R.E. DeVor, An experimental investigation of the crack growth phenomenon for drilling of fiber-reinforced composite materials, J. Eng. Ind. 118 (1996) 104–110.
[27] G.P. Zhu, Y.J. Bao, H. Gao, Research on the drilling temperature field model of the unidirectional carbon fiber epoxy composites, Adv. Mater. Res. 565 (2012) 478–483.
[28] A. Sadek, B. Shi, M. Meshreki, J. Duquesne, M.H. Attia, Prediction and control of drilling-induced damage in fibre-reinforced polymers using a new hybrid force and temperature modelling approach, CIRP Ann. - Manuf. Technol. 64 (2015) 89–92.
[29] J. Díaz Álvarez, A. Olmedo, C. Santiuste, M.H. Miguélez, Theoretical estimation of thermal effects in drilling of woven carbon fiber composite, Materials 7 (2014) 4442–4454.
[30] C. Bonnet, G. Poulachon, J. Rech, Y. Girard, J.P. Costes, CFRP drilling: Fundamental study of local feed force and consequences on hole exit damage, Int. J. Mach. Tool Manufact. 94 (2015) 57–64.
[31] T. Yashiro, T. Ogawa, H. Sasahara, Temperature measurement of cutting tool and machined surface layer in milling of CFRP, Int. J. Mach. Tool Manufact. 70 (2013) 63–69.
[32] M. Vollmer, M.Ã. Klaus-Peter, Infrared thermal Imaging: Fundamentals, Research and Applications, second ed., John Wiley & Sons, Weinheim, 2017.
[33] D. Biermann, F. Hollmann, Thermal Effects in Complex Machining Processes: Final Report of the DFG Priority Programme 1480, Springer, Cham, 2017.
[34] C.Y. Wang, Y.H. Chen, Q.L. An, X.J. Cai, W.W. Ming, M. Chen, Drilling temperature and hole quality in drilling of CFRP/aluminum stacks using diamond coated drill, Int. J. Precis. Eng. Manuf. 16 (2015) 1689–1697.
[35] M. Sato, T. Aoki, H. Tanaka, S. Takeda, Measurement of temperature at bottom surface of hole in drilling of CFRP and titanium stack, Proc. Int. Conf. Lead. Edge Manuf. 21st Century LEM21 2013, vol. 7, 2013, pp. 448–451.
[36] J.L. Merino Pérez, R. Royer, S. Ayvar Soberanis, E. Merson, A. Hodzic, On the temperatures developed in CFRP drilling using uncoated WC-Co tools Part I: workpiece constituents, cutting speed and heat dissipation, Compos. Struct. 123 (2015) 161–168.
[37] F. Makhdum, V.A. Phadnis, A. Roy, V.V. Silberschmidt, Effect of ultrasonically-assisted drilling on carbon-fibre-reinforced plastics, J. Sound Vib. 333 (2014) 5939–5952.
[38] P.W. Butler-Smith, D.A. Axinte, M. Daine, A.R. Kennedy, L.T. Harper, J.F. Bucourt, R. Ragueneau, A study of an improved cutting mechanism of composite materials using novel design of diamond micro-core drills, Int. J. Mach. Tool Manufact. 88 (2015) 175–183.
[39] M.R. Choudhury, M.S. Srinivas, K. Debnath, Experimental investigations on drilling of lignocellulosic fiber reinforced composite laminates, J. Manuf. Process. 34 (2018) 51–61.
[40] D. Geng, Z. Lu, G. Yao, J. Liu, Z. Li, Cutting temperature and resulting influence on machining performance in rotary ultrasonic elliptical machining of thick CFRP, Int. J. Mach. Tool Manufact. 123 (2017) 160–170.
[41] M.A.R. Loja, M.S.F. Alves, I.M.F. Bragança, R.S.B. Rosa, I.C.J. Barbosa, J.I. Barbosa, An assessment of thermally influenced and delamination-induced regions by composites drilling, Compos. Struct. (2018), https://doi.org/10.1016/j.compstruct.2018.02.046.
[42] Infrared Camera Blackbody Free Calibration Technique, (2018) http://info.telops.com/Website-content-requests_05—LP—Infrared-Camera-Blackbody-Free-Calibration-Technique.html , Accessed date: 28 June 2018.
[43] M. Akay, Aspects of dynamic mechanical analysis in polymeric composites, Compos. Sci. Technol. 47 (1993) 419–423.
[44] Y. Miyano, M. Nakada, N. Sekine, Accelerated testing for long-term durability of FRP laminates for marine use, J. Compos. Mater. 39 (2005) 5–20.
[45] Z. Jia, Y. Su, B. Niu, B. Zhang, F. Wang, The interaction between the cutting force and induced sub-surface damage in machining of carbon fiber-reinforced plastics, J. Reinforc. Plast. Compos. 35 (2016) 712–726.
[46] Z. Jia, R. Fu, B. Niu, B. Qian, Y. Bai, F. Wang, Novel drill structure for damage reduction in drilling CFRP composites, Int. J. Mach. Tool Manufact. 110 (2016) 55–65.
[47] F. Girot, F. Dau, M.E. Gutiérrez-Orrantia, New analytical model for delamination of CFRP during drilling, J. Mater. Process. Technol. 240 (1) (2017) 332–343.
[48] F. Wang, B. Qian, Z. Jia, R. Fu, D. Cheng, Secondary cutting edge wear of one-shot drill bit in drilling CFRP and its impact on hole quality, Compos. Struct. (2017) 1–12.
[49] Weixing Xu, L.C. Zhang, Mechanics of fibre deformation and fracture in vibration-assisted cutting of unidirectional fibre-reinforced polymer composites, Int. J. Mach. Tool Manufact. 103 (2016) 40–52.
[50] S. Nak-Ho, N.P. Suh, Effect of fiber orientation on friction and wear of fiber reinforced polymeric composites, Wear 53 (1979) 129–141.
[51] D.W. Hahn, M.N. Özışık, Heat Conduction, third ed., John Wiley & Sons, Hoboken, 2012.
[52] A. Sanda, I. Arriola, V. Garcia Navas, I. Bengoetxea, O. Gonzalo, Ultrasonically assisted drilling of carbon fibre reinforced plastics and Ti6Al4V, J. Manuf. Process. 22 (2016) 169–176.
[53] V. Madhavan, G. Lipczynski, B. Lane, E. Whitenton, Fiber orientation angle effects in machining of unidirectional CFRP laminated composites, J. Manuf. Process. 20 (2015) 431–442.
[54] X.J. Cai, Experimental Study on Cutting Force and Heat Variation and Surface Quality Evaluation Based on Anisotropy of Composites, Ph.D. thesis Shanghai Jiao Tong University, 2014.
[55] O. Gavalda Diaz, D.A. Axinte, Towards understanding the cutting and fracture mechanism in Ceramic Matrix Composites, Int. J. Mach. Tool Manufact. 118 (2017) 12–25.
[56] X.M. Wang, L.C. Zhang, An experimental investigation into the orthogonal cutting

of unidirectional fibre reinforced plastics, Int. J. Mach. Tool Manufact. 43 (2003) 1015–1022.

Rao Fu has a Ph.D. in Mechatronic Engineering from Dalian University of Technology. He is currently a research fellow within the School of Mechanical and Aerospace Engineering, at Queen's University Belfast. His research interests focus on the low-damage drilling CFRP, cutting tool design and machining error propagation with parallel kinematic machine.

Zhenyuan Jia has a Ph.D. in Mechanical Engineering from Dalian University of Technology. He is currently a professor within the Key Laboratory for Precision and Non-traditional Machining Technology of the Ministry of Education, School of Mechanical Engineering, Dalian University of Technology. His research interests are mainly in theory and technology for high quality and high efficient machining of CFRP composite, precision measurement and control of manufacturing process, numerical control technique, and applications of smart material in sensors and actuators.

Fuji Wang has a Ph.D. in Mechanical Engineering from Dalian University of Technology. He is currently a professor within the Key Laboratory for Precision and Non-traditional Machining Technology of the Ministry of Education, School of Mechanical Engineering, Dalian University of Technology. His research interests include high quality and efficient machining processing of CFRP, high precision numerical control technique, unconventional manufacturing processes.

Yan Jin has a Ph.D. in Mechanical Engineering from Nanyang Technological University Singapore. He is currently a reader within the School of Mechanical and Aerospace Engineering, at Queen's University Belfast. Dr Jin has broad research interests mainly in parallel kinematic machines, robotics automation, digital lean manufacturing, high performance machining and production management.

Dan Sun has a Ph.D. in Mechanical Engineering from University of Southampton. She is currently a lecturer at Queen's University Belfast and is affiliated to the Advanced Composite Research Group within the School of Mechanical and Aerospace Engineering. Dr Sun has broad research interests and a wide spectrum of expertise in areas of synthesis and processing of polymer-based composites, manufacturing and characterization of aircraft materials, surface engineering and tribology, etc.

Lujia Yang has a Ph.D. in Design and Manufacture of Ship and Ocean Structure from Dalian University of Technology. She is currently a lecturer within the School of Innovation and Entrepreneurship, Dalian University of Technology. Her research focuses on the innovative design of robot, data processing technology, machining technology and corrosion prevention.

De Cheng is a master student at School of Mechanical Engineering, Dalian University of Technology. His master research topic is focused on the low-damage drilling process for CFRP composites.